Magnetic remanent states and magnetization reversal in patterned trilayer nanodots

K. S. Buchanan,[1,*] K. Yu. Guslienko,[1] A. Doran,[2] A. Scholl,[2] S. D. Bader,[1] and V. Novosad[1]
[1]*Materials Science Division and Center for Nanoscale Materials, Argonne National Laboratory, 9700 South Cass Avenue, Argonne, Illinois 60439, USA*
[2]*Lawrence Berkeley National Laboratory, 1 Cyclotron Road, Berkeley, California 94720, USA*
(Received 7 February 2005; revised manuscript received 10 August 2005; published 14 October 2005)

The magnetic properties of a trilayer system involving two ferromagnetic disks separated by a nonmagnetic spacer differ from those of isolated dots due to the magnetostatic and interlayer exchange coupling across the spacer. The reversal process for this system has been investigated experimentally, analytically and numerically for permalloy ($Ni_{80}Fe_{20}$) dots with thicknesses of up to 40 nm and radii of 0.25–1.25 μm separated by a Cu spacer up to 45 nm thick. Hysteresis measurements and photoemission electron microscopy images of the remanent states show evidence of the vortex remanent state and reversal, respectively. Single and multidomain states, however, can be stabilized through flux closure between layers resulting in a reduction of the phase space occupied by the vortex state. Micromagnetic simulations indicate that the disks will each support oppositely directed vortices at remanence that reverse through coordinated nucleation, displacement and annihilation of vortices in the two layers. Experimental and numerical magnetic susceptibilities are in agreement with analytical calculations based on the rigid vortex model.

DOI: 10.1103/PhysRevB.72.134415 PACS number(s): 75.75.+a, 75.60.Jk, 75.30.Kz

INTRODUCTION

The magnetic properties of submicron structures (dots) can be dramatically different than for bulk materials. Magnetically soft dots in particular have received considerable attention due to their tendency to support a stable vortex magnetization state.[1–7] The properties of the vortex state have thus far been examined mainly for uncoupled dots,[1,3] or else for weakly interacting dots of different shape arranged on a 2D surface.[2,8–11] For structures consisting of two ferromagnetic cylindrical dots separated by a thin, nonmagnetic spacer (F/N/F), however, the F layers will be strongly coupled through magnetostatic interactions, which can have an effect on the remanent state and the magnetization reversal process. In addition, interlayer exchange coupling can play an important role, depending on the thickness and composition of the spacer layer. Py/Cu multilayers, for example, are known to exhibit giant magnetoresistance (GMR) and show oscillatory bilinear exchange coupling with a peak GMR signal for a spacer thickness of 0.9 nm. GMR ratios as high as 20% have been reported for sputtered Py/Cu multilayers.[12] The trilayer F/N/F system is of fundamental interest due to the strong interactions between the dots and the variety of possible magnetization states and is of technological interest for applications such as magnetic sensors or magnetic random access memory (MRAM), especially for dots fabricated using GMR multilayers.

Previously, combined experimental, numerical and analytic approaches have been used to determine the conditions necessary for a single-layer disk to support a vortex and to explore the hysteretic switching through vortex nucleation, displacement and annihilation.[1–3] In arrays of well-separated magnetically soft submicron and micron diameter dots the magnetic susceptibility χ and annihilation field H_a have been shown to depend only on the dot aspect ratio thickness/radius $\beta=L/R$ and the saturation magnetization M_s in a predictable manner,[1] confirming that the magnetostatic energy dominates over the exchange energy. The effect of the magnetostatic coupling between magnetic particles is important for closely spaced dots but this has mainly been explored for dots arranged on a two-dimensional (2D) surface. The interactions for this geometry have led to increased magnetic susceptibilities,[2] have an effect on the dynamic excitation spectra of the dots,[8] and may also lead to correlated vortex chirality in neighboring elements.[9–11] Strong dynamic magnetostatic interaction effects on the vortex eigenfrequencies and core trajectories were predicted recently.[13] Monte Carlo simulations have been used to investigate trilayered rectangular elements and predict vortex formation in one layer but not the other.[14] However, the magnetization reversal mechanisms for trilayered dots are not yet well understood.

In this paper, the effects of interactions on magnetization reversal are explored for trilayer magnetic dots. The problem is approached analytically, numerically and experimentally. Arrays of trilayer F/N/F structures were fabricated using electron beam lithography and magnetron sputtering followed by a lift-off process. The hysteresis curves were measured using the magneto-optical Kerr effect and the remanent states of the patterned structures were imaged using x-ray photoemission electron microscopy. Micromagnetic simulations were carried out to gain insight into the field evolution of the magnetization distribution and the conditions necessary to favor the vortex magnetization state in both F layers. Analytical calculations of the magnetic susceptibility and the ground state phase diagram based on the rigid vortex model have been compared to experimental and numerical results.

EXPERIMENTAL DETAILS

Patterned arrays of trilayer circular dots (1.2–2.5 μm in diameter) were fabricated on silicon wafers using electron beam lithography and liftoff with ZEP520A high-sensitivity positive tone resist.[15] Layers of permalloy ($Ni_{80}Fe_{20}$ or Py) of

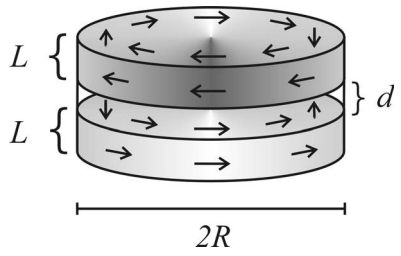

FIG. 1. Illustration of the double vortex state for two magnetic circular dots of thickness L and diameter $2R$ separated by a nonmagnetic spacer of thickness d.

identical thickness (20–40 nm thick) separated by copper with variable thicknesses of 1–20 nm were grown with magnetron sputtering. The in-plane hysteresis loops of the patterned arrays were measured in the transverse magneto-optical Kerr effect (MOKE) geometry at a wavelength of 532 nm and an angle of incidence of 45°. The change of intensity of the reflected beam is directly proportional to the component of the magnetization perpendicular to the plane of incidence and is recorded as a function of the in-plane magnetic field. For patterned arrays, the MOKE technique is convenient because hysteresis measurements can be made from smaller arrays (100×100 μm or less) than are needed for SQUID measurements. Unlike inductive methods, the MOKE technique will probe the magnetization state within the depth penetration of the light (i.e., only the surface of layered structures).

Magnetic domain imaging was carried out using the photoemission electron microscope (PEEM-2) at beamline #7.3 of the Advanced Light Source. This microscope is capable of probing the magnetization state at remanence with spatial resolution of <100 nm.[16] The sample is illuminated with monochromatic, circularly polarized x rays tuned to the L_2 (870.0 eV) and L_3 (852.7 eV) Ni absorption edges.[17] The difference in the absorption between x rays of each polarization is proportional to the magnetization of the sample in the scattering plane and yields the magnetic circular dichroism (MCD) signal that is detected by monitoring the photoemission of electrons from the sample; the ratio of the intensities of the images taken at the L_2 and L_3 edges provides the final image. For samples examined using PEEM, the substrate was coated with a thin layer of Cr/Au prior to patterning to ensure electrical conductivity and the disks were overcoated with an additional 1 nm of Pd to protect them from oxidation.

ANALYTICAL CALCULATIONS

Here we describe analytically the magnetic phase diagram and the magnetic susceptibility for F/N/F dots. The magnetic phase diagram was calculated by determining the lowest energy regions for expected remanent states, while the magnetic susceptibility was evaluated by determining the displacement of the vortex magnetization state in response to a small external magnetic field. Figure 1 illustrates the geometry of the trilayer dots (the F/N/F structure) with diameter $2R$, spacer thickness d, and identical magnetic layer thicknesses L. With the $\hat{z}$ axis directed parallel to the dot cylindrical axis, the reduced magnetization $\mathbf{m}=\mathbf{M}/M_s$ components can be described by $m_z=\cos\Theta$, and $m_x+im_y=\sin\Theta\exp(i\Phi)$, where the spherical angles Θ and Φ of $\mathbf{m}$ are functions of the cylindrical coordinates (ρ,φ). All quantities were averaged over the dot thickness. For the vortex-like magnetization distribution in a cylindrical dot, the equation $\Phi=\varphi+\nu\pi/2$ corresponds to the condition of zero volume magnetic charges ($m_\rho=0$), and it is assumed that the function $\Theta=\Theta(\rho)$ is axially symmetric for a centered vortex.[1] The area with $\Theta(\rho)\neq\pi/2$ is the vortex core. The "winding" index $\nu=\pm1$ (chirality) corresponds to counterclockwise or clockwise magnetization rotation around the dot center, respectively. The field dependence of the micromagnetic exchange energy is neglected assuming the micron-size dot radii R is much greater than the micromagnetic exchange length l_{ex} defined as $l_{\mathrm{ex}}=\sqrt{2A}/M_s$, where A is the exchange stiffness constant, and M_s is the saturation magnetization.

The magnetostatic energy contribution within the vortex model arises from the surface magnetic charges $\sigma=(\mathbf{M}\cdot\mathbf{n})$:

$$W_m=\frac{1}{2}\int dS\int dS'\frac{\sigma(\mathbf{r})\sigma(\mathbf{r}')}{|\mathbf{r}-\mathbf{r}'|},\qquad(1)$$

where the integration is over the surface S of the dot. Volume charges are absent ($\mathrm{div}\,\mathbf{m}=0$) due to the assumptions that $m_\rho=0$ and $m_\varphi=m_\varphi(\rho)$. The dot magnetostatic energy (1) for the face (due to the m_z component, which is nonzero for the vortex cores) and side surface charges induced by applying an in-plane magnetic field should be calculated separately. The face charges are responsible for the magnetostatic interaction of the vortex cores, however, both analytical and numerical calculations show that this energy term is very small for micron dot radii and can be neglected in considering the F/N/F in-plane hysteresis. The state with the same core polarizations has a slightly lower energy for centered vortices.

A ground-state phase diagram can be calculated by comparing the energy expression for the double vortex state (centered vortices in each F layer) to that of a coupled, single-domain (SD) state following the method used to calculate the phase diagram for single-layer magnetic dots.[18] Vortices normally form to reduce the magnetostatic energy in a single dot but, as we show below, when there are two disks stacked vertically, the energy of the SD state can be reduced through magnetic flux closure between antiparallel layers. For this case the magnetostatic interaction energy depends strongly on the thickness of the separating layer d and can be expressed (in units of M_s^2V, where $V=2\pi R^2L$ is the dot magnetic volume) as

$$w_{\parallel}(\beta,d/R)=2\pi[F_1(\beta)-F_{\mathrm{int}}(\beta,d/R)],$$

$$F_{\mathrm{int}}(\beta,d/R)=\frac{1}{2\beta}\int_0^\infty dte^{-td/R}(1-e^{-\beta t})^2\frac{J_1(t)^2}{t^2},\qquad(2)$$

where $J_1(t)$ is the first-order Bessel function, and $F_1(\beta)=\int_0^\infty dt[1-(1-e^{-\beta t})/\beta t]J_1(t)^2/t$, $\beta=L/R$.

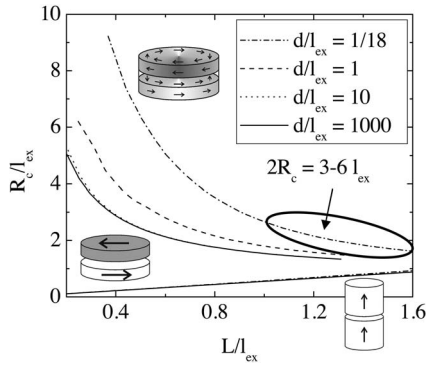

FIG. 2. Magnetic phase diagram for trilayer F/N/F cylindrical dots for spacer thicknesses ranging from the single dot limit down to $l_{ex}/18$ or 1 nm. For the F layers and spacer thicknesses considered here the critical diameter $2R_c$ is $6l_{ex}$ or less.

The energy density of the centered double vortex state, neglecting the core-core interaction and interlayer exchange, is equal to the energy density $w_v(L,R)$ of a single disk in the vortex state, independent of the chiralities of the two vortices. At remanence there are no stray fields in the centered vortex model, apart from at the cores, that would lead to an interlayer interaction energy term. The single vortex energy density was calculated in Ref. 19 by minimizing the sum of exchange and magnetostatic energies and considering the vortex core radius as an adjustable parameter. For thick enough cylindrical dots ($L \geqslant l_{ex}$) the energy density is $w_v(L,R)=(l_{ex}/R)^2[7/3-\ln(\xi L^{1/3} l_{ex}^{2/3}/R)]$, where $\xi \approx 0.68$. This expression is valid for large enough dot radius R, whereas essential deviations from the vortex core profile[19] and vortex energy were calculated for small $R \approx l_{ex}$ in Ref. 20. The vortex energy density[19] results in the following equation for the critical radius $R_c(L,d)$ separating the antiparallel SD ground state with in-plane magnetization from the double vortex ground state, $w_{\parallel}(L/R,d/R)=w_v(L,R)$, shown in Fig. 2. Note that the magnetizations in the F layers are antiparallel for both the SD and vortex states.

If R is kept constant and L is increased, there is an energy minimum for the state with perpendicular magnetizations in each layer. Its energy density is

$$w_{\perp}(\beta,d/R) = \tfrac{1}{2}N_z(\beta) - 4\pi p_1 p_2 F_{\text{int}}(\beta,d/R), \tag{3}$$

where N_z is the single disk demagnetizing factor in the z-direction, p_j defines the magnetization direction in the jth layer. Assuming $p_1 p_2 = 1$ and using the well known relations of the averaged demagnetizing factors for circular cylinders $2N_x(\beta)+N_z(\beta)=4\pi$ and $N_x(\beta)=4\pi F_1(\beta)$ along with the equality $w_{\parallel}(\beta,d/R)=w_{\perp}(\beta,d/R)$, the equation for the critical line of transition between the in-plane and out-of-plane SD states can be expressed in the simple form,

$$3F_1(\beta) + F_{\text{int}}(\beta,d/R) = 1. \tag{4}$$

Equation (4) has a solution in the form of a scaling function $\beta_c(d/R)$ that depends explicitly on the interlayer coupling. For $d/R \gg 1$ the function approaches the value 1.81 calculated by Aharoni[21] for a single layer disk. For vanishing interlayer separation $d \to 0$ the function approaches its limiting value $\beta_c(0)=1.47$.

The magnetic phase diagram for selected spacer separation values is illustrated in Fig. 2 for Py using $M_s = 800$ emu/cm^2. Above the critical radius R_c the vortex state has the lowest energy. The double-vortex and antiparallel SD magnetization states will also have overlapping regions of stability (first order phase transition line on the phase diagram). The vortex state stability line was calculated for single-layer circular dots in Ref. 22 and the area of metastability of vortex/SD states in thin dots was probed in Ref. 23. The geometrical parameters of the disk are normalized by the magnetic exchange length l_{ex} and, therefore, this diagram is universal for all soft magnetic materials.[24] The analytical calculations show that increasing the magnetostatic coupling between the disks will result in a reduction of the phase space occupied by the vortex state. The energy of the SD state is reduced due to the flux closure between the layers. This effect is most pronounced when the separation is $\leqslant l_{ex}$; for $d \geqslant 10 l_{ex}$, the phase diagram approaches the single disk limit. The change to the perpendicular/in-plane phase boundary is small for $d \geqslant 1$ nm. All of the phase space explored experimentally falls in the region where the double vortex state has the lowest energy. It is important to note, however, that the lowest energy state may not always be accessible depending on the magnitude of the nucleation barrier.[23]

To calculate the response of the double vortex state in an external in-plane magnetic field, a "rigid vortex" model was used.[1] As the name implies, this model assumes that the core position shifts from the dot center with no deformation of the magnetization distribution when a field is applied. For this model the field-induced, side-surface magnetic charges play an important role in determining the vortex state susceptibility as described below. The size and field dependence of these charges and the corresponding magnetostatic energy for single-layer dots were reported earlier.[1,18] Using a similar approach, the total magnetic energy density of the F/N/F dot with shifted vortices, including the magnetostatic coupling energy between two F layers, the energy of the system in a non-zero external field can be expressed as

$$w(s) = w(0) + 2\pi[F_1(\beta) + F_{\text{int}}(\beta,d/R)]s^2 - \frac{1}{2}\left(\frac{l_{ex}}{R}\right)^2 s^2 - hs, \tag{5}$$

where $s=l/R$ is the relative vortex core shift from the dot center in the direction perpendicular to the external applied in-plane field and $h=H/M_s$ is the reduced magnetic field. In this case the interaction term F_{int} is positive as it comes mainly from dot side surface charges of the same sign, whereas in Eq. (2) the coupling energy is negative because single domain states with oppositely oriented magnetizations were assumed, resulting in surface charges of opposite sign.

The initial susceptibility χ and vortex annihilation (saturation) field H_{an} of the F/N/F structure can be calculated by minimizing the total magnetic energy with respect to field in the limit of small h. For different signs of the layer chiralities, corresponding to an initial (zero-field) "antiferromagnetic" magnetization state, a symmetric separation of the

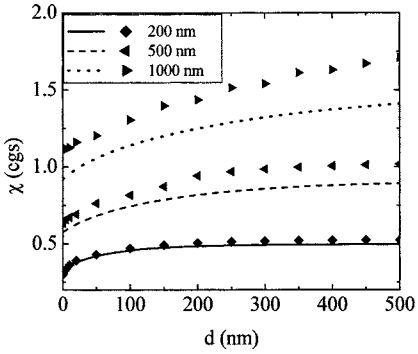

FIG. 3. Analytic (lines) and numerical (symbols) calculations of the initial magnetic susceptibility of the double vortex state in trilayer F/N/F dot as a function of spacer thickness. Each line/symbol type represents a different diameter.

vortex cores in response to an applied field is expected for identical thicknesses of the F layers. If the chiralities are the same the cores will shift in the same direction when a field is applied, however, in the quadratic approximation in s used here, χ and H_{an} for both cases are the same. Neglecting the exchange contribution and defining the auxiliary function $a(\beta,d/R)=2\pi[F_1(\beta)+F_{\mathrm{int}}(\beta,d/R)]$ (see Ref. 1), χ and H_{an} can be calculated from Eq. (5) as

$$\chi(\beta,d/R)=\tfrac{1}{2}a^{-1}(\beta,d/R), \quad H_{an}(\beta,d/R)=2a(\beta,d/R)M_s. \tag{6}$$

The influence of interdot magnetostatic coupling on χ and H_a was studied earlier for single-layer circular dots arranged in 2D planar arrays.[2] In that study χ, which is a measure of the in-field vortex stability, the nucleation field H_n, and H_{an} were reported to scale as a function of the interdot distance normalized to the dot radius d/R. This is similar to the case of patterned trilayers considered here. Figure 3 shows a how χ [Eq. (6)] increases as a function of d, approaching the value for a single disk for $d\sim D$. Conversely, χ decreases as a function of the aspect ratio β.

The calculations above have neglected the effects of interlayer exchange interactions. However, antiferromagnetic (AF) interlayer exchange is expected to favor the formation of both the opposite chirality double-vortex and the coupled antiparallel SD states, acting as an effective increase in the magnetostatic coupling between the layers, whereas ferromagnetic interlayer coupling, in contrast, would expand the stability region of SD and vortex states with parallel spin alignment in the neighboring layers.

MICROMAGNETIC MODELING

Micromagnetic simulations were conducted using a Landau-Lifshitz-Gilbert solver[25] to gain insight into the field evolution of the magnetization reversal process and the remanent states for the F/N/F disks. For the calculations, Py dots were defined with L of 15 to 40 nm, R of 0.25 and 0.5 μm, and d of 1 to 45 nm. Bulk Py values for M_s (800 emu/cm^3) and A (1.05×10^{-6} erg/cm) were used and the magnetocrystalline anisotropy was neglected. The hysteresis loops were

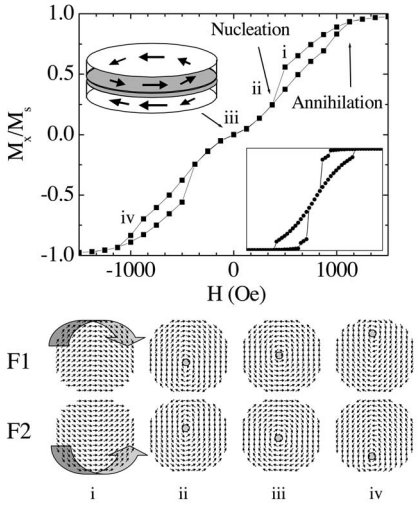

FIG. 4. Simulated hysteresis curve for a 500-nm diameter dot with 20-nm thick Py layers separated by a 1 nm thick nonmagnetic spacer with the interlayer exchange coupling field of −250 Oe. The micromagnetic magnetization distributions indicate that the spins in each layer curl at the edges as the field is reduced from saturation, taking on configurations similar to the letter "C" but in opposing directions in the two layers, F1 and F2. As the field is reduced further, vortices of opposite chirality nucleate at opposite edges, reach the disk center at zero field, then separate and annihilate at the other edges. The inset shows how the simulated hysteresis curve differs for a ferromagnetic interlayer exchange field (H_J= +250 Oe).

simulated by relaxing the system under sequentially applied magnetic fields to approximate a progression of equilibrium states, and simulations of the remanent state were carried out by allowing the system to relax from saturation in the absence of an applied field. For all simulations a large damping parameter was used ($\alpha\sim0.8$).

Figure 4 shows a representative hysteresis curve and the associated field dependent magnetization distributions simulated for $2R$=500 nm, L=20 nm Py disks with d=1 nm and an interlayer exchange field of H_J=−250 Oe (defined from the expression for surface exchange energy density $w_{\mathrm{ex}}=-H_J\cdot ML$). The shape of the in-plane hysteresis curve for this trilayer structure is similar to that of a single disk reversing through a single vortex process. When the magnetic field is reduced from saturation, vortices nucleate at opposing edges of the upper and lower disks and then move until they reach the disk edges and are annihilated. The cores move in opposite direction toward the disk edges as the magnetic field is changed such that the magnetization vectors for both disks are parallel to the applied field in the central region. At remanence the F/N/F disk supports the centered double vortex state. From saturation, the magnetization of the disks decreases more than for a single disk prior to vortex nucleation corresponding to curling of the magnetization of each layer such that the magnetization follows the shape of the letter "C" (often referred to as a C-state[1,18,26]) in one layer and its reflection in the other. If the field is kept below the annihilation field then reversible displacement of the vortices is observed. For ferromagnetic interlayer exchange (inset of

Fig. 4 shows simulation for $H_J=+250$ Oe), the layer magnetizations still curl in opposing "C" states due to the strong magnetostatic coupling, however, vortices nucleate at a higher field and have the same chiralities.

In the simulation in Fig. 4 the opposing chiralities are favored partially by the inclusion of antiferromagnetic interlayer exchange, however, for $L=40$ nm and $d=1$ nm a similar reversal mechanism is observed with no interlayer exchange. In general, only the opposite chirality state was observed in the simulations. This configuration is slightly lower in energy than the same chirality state in the numerical models. For the analytical rigid vortex model there is no energy difference but in the simulations the magnetization distribution has a nonzero radial component near the core that induces volume charges and provides a mechanism for magnetostatic interactions between the disks[18] and there are also discretization effects at the dot edges. In the hysteresis simulations the layer magnetizations curl in opposite directions in the two layers because this avoids the accumulation of same-sign magnetic surface charges at the same x-y positions that would result if both layers curled in the same direction. Thus the consistent observation of the opposite chirality states in the simulations likely reflects an energy difference in the nucleation process rather than the small energy difference between the final states. In most simulations the core polarizations were oriented in the same direction; however, the energy difference is small. For $L=40$ nm, $d=1$ nm, $2R=1$ μm, and $H_J=0$, the same core polarization configuration is only lower in energy by $\sim 4\%$ and this energy difference is only significant when the vortex cores are close together. Based on the simulation results the opposite chirality state is expected to dominate; however, other core polarization combinations are likely. Correlated vortex chiralities have been reported for strongly coupled dotes arranged in planar arrays.[9,11]

The micromagnetic simulations indicate that the disks will usually support centered vortices with opposing chiralities at remanence, however, this state was not observed for all parameter combinations even if the analytical calculations indicate that the double vortex is the lowest energy state. For example, the simulations indicate that two $L=15$ nm, $2R=500$ nm disks, separated by $d=1$ nm, will settle into antiparallel, SD states when the sole source of coupling is magnetostatic. Thus it will be important to consider not only the energy of the final state for this system but also the accessibility of that state, i.e., the nucleation mechanism and associated energy barriers.[23] A number of simulations were carried out to gain insight into what conditions would favor the double vortex state. Parameters that were varied include M_s, $2R$, L, d, and H_J.

Increasing L, or M_s leads to an increase in the magnetostatic energy contribution, which energetically favors the vortex state for a single disk, and consequently increases the likelihood of observing the double vortex state in a F/N/F dot at remanence. Similarly, an increase in H_J (AF), will promote the nucleation of vortices with opposite chirality. Increasing d can also favor the double vortex state because this will reduce the energy savings provided by flux closure between the layers that can impede the vortex nucleation. Using $2R=500$ nm, $L=15$ nm, and $d=1$ nm as a starting point

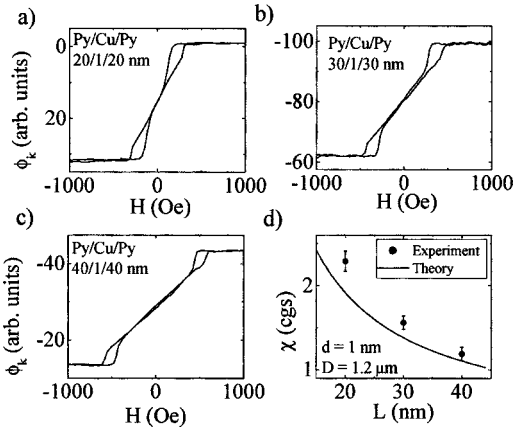

FIG. 5. In-plane MOKE hysteresis curves for 1.2-μm-diameter Py disks separated by 1 nm of Cu for Py thicknesses of (a) 20 nm, (b) 30 nm, and (c) 40 nm. All exhibit vortex-like magnetization reversal. (d) A comparison of the measured susceptibility with the analytic predictions (6) as a function of the F layer thickness.

($H_J=0$), increasing L to 40 nm resulted in a stable double vortex. Keeping L at 15 nm and increasing d similarly resulted in double vortices. For $d=30$ nm the vortices formed but were off-center, whereas for $d=45$ nm centered vortices were observed. Increasing M_s resulted in greater curling of the magnetization, however, M_s of 1700 emu/cm^3 (iron), was not sufficient to induce centered vortices. Increasing H_J (AF) also has a stabilizing effect. Disks 20 nm thick with $d=1$ nm, for example, did not support vortices for $H_J=0$ but with $H_J=-250$ Oe, AF vortices are stable. For $L=20$ nm a minimum d of between 20 and 40 nm is required to allow nucleation of the double vortex state even though the energy for the vortex state is lower for all separations.

The variation of χ as a function of d was modeled for d ranging from 1 to 500 nm and $2R$ of 200, 500, and 1000 nm (Fig. 3) by simulating the change in magnetization of the double vortex state for a small in-plane bias field (100 Oe). χ increases as a function of d following the shape of the analytic predictions of Eq. (6), approaching the single-disk value for $d>2R$. The simulated and analytic calculation results compare well for small disk diameters, however, the theory underestimates the simulation results for χ as $2R$ increases. These discrepancies may be related to the fact that the rigid vortex model is less appropriate for larger disks where the vortex has more flexibility to deform as it moves across the disk to minimize stray fields.

EXPERIMENTAL RESULTS

Trilayer Py/Cu/Py disks were patterned with diameters of 1.2, 1.5, 2, and 2.5 μm and Py thicknesses of 20, 30, and 40 nm using a constant Cu spacer thickness of 1 nm. This d-value was chosen as it is near the AF peak of the interlayer exchange coupling. A set of disks with 20 nm of Py separated by 20 nm Cu was also prepared in order to compare results for a case with strong magnetostatic interactions but negligible interlayer exchange. The in-plane hysteresis curves for the samples with a 1-nm spacer (Fig. 5) show

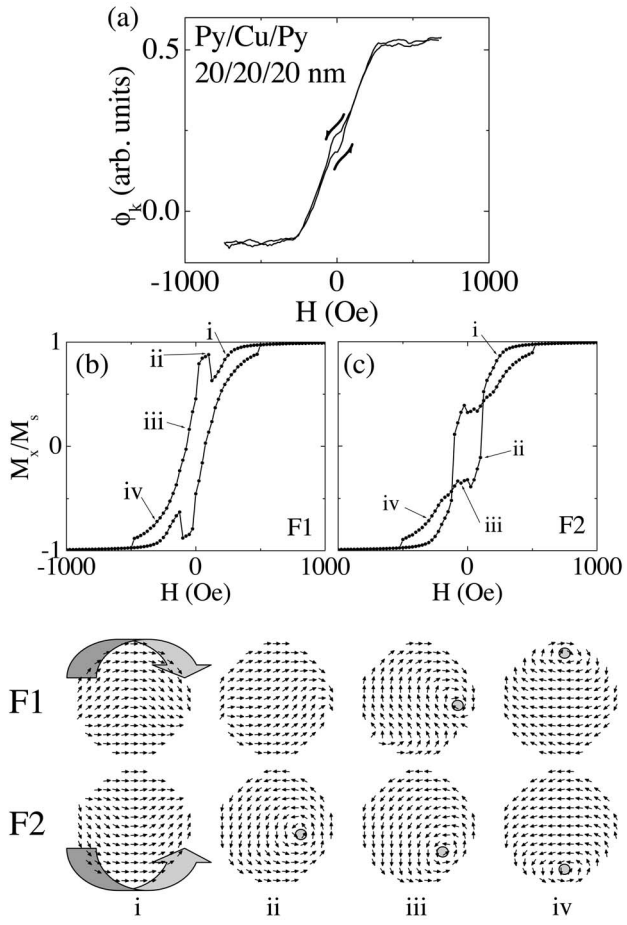

FIG. 6. (a) MOKE hysteresis for the 20/20/20 nm dots, diameter 1.2 μm indicates that this sample does not follow the double vortex reversal process illustrated in Fig. 2. Simulated hysteresis loops for this parameter combination are shown in (b) and (c) for each F layer and the corresponding magnetization distributions are shown below. As the field is reduced from saturation the layers curl in opposing directions. A vortex nucleates first in layer F1 (ii), and then in the layer F2 (iii) only after passing through zero field. The vortices annihilate at opposite edges in the two layers, remaining near the dot edge from inception to annihilation.

evidence of a vortex reversal mechanism, although the nucleation is more abrupt as compared to the shape of the simulated hysteresis curve (Fig. 4). This discrepancy may be related to differences in the magnitude of J. It may also indicate that there is direct exchange coupling between the Py layers due to either roughness at the film interface or else contact at the dot edges. Further investigation will be needed to probe the state of the bottom layer. The size of the side-lobes of the experimental loops and χ both decrease as a function of increasing Py thickness. The magnetic susceptibility trend is qualitatively consistent with the theoretical prediction [Eq. (2)] as shown in Fig. 5(d), however, the analytical model underestimates the actual values by an amount similar to the discrepancy with the simulations for the 1-μm diameter disks.

The hysteresis curve for the Py/Cu/Py 20/20/20 nm specimen, shown in Fig. 6, is much different in shape. The side-lobes characteristic of the nucleation/annihilation process are absent and instead a small non-zero coercivity is observed in a loop that otherwise resembles that of a coherent rotation reversal. Micromagnetic simulations of the hysteresis for the "top" and "bottom" layers (Fig. 6) for $2R=1.2$ mm and $L=d=20$ nm suggest an alternative interpretation. In the simulations, both layers display hysteresis loops with a boxlike feature in the center. Unlike the double-vortex reversal simulations, however, the individual layers show different hysteresis curves and spin distributions. At high magnetic fields the curves coincide but as the field is reduce the curves diverge. A vortex forms first in the "bottom" layer at a positive nucleation field (100 Oe), resulting in an abrupt drop its magnetization. This drop coincides with a temporary increase (i.e., straightening) of the top layer magnetization. At remanence, one layer supports a vortex at its edge while the other is primarily single-domain with some curling of the magnetization distribution. The vortex in the "top" layer, once formed, travels along the dot edge. At a field of -50 Oe, after passing through zero, a vortex nucleates in the top layer and then it also travels along the dot edge. The vortices have opposite chiralities and annihilate at opposite edges of the dot at almost the same field. The MOKE technique is sensitive primarily to the top layer of the experimental sample; however, it measures the hysteresis of a large array of dots and the choice of "top" and "bottom" in the simulations is arbitrary as the layers are identical. The simulated curves are more open than the data but overall the experimental curve is similar to an average of the simulated loops biased slightly towards the "top" reversal mode.

The magnetization distributions for the samples were imaged in zero field using PEEM. Representative images of the trilayer disks are shown in Fig. 7. The intensity of the contrast is directly proportional to the dot product of the magnetization vector and the propagation direction of the x rays. Figure 7(a) shows an image of the 20/1/20 nm sample after fabrication before any magnetic fields were applied. This image shows that the top layers of all of the disks are in the vortex magnetization state. During fabrication the first layer of Py can take on a single-vortex magnetization state directly after deposition. This first layer then influences the magnetization state of the second layer as it is being deposited, resulting in the double vortex state. After saturating the sample (along the in-plane direction of illumination) and returning to remanence, most of the dots relax back into a vortex state, although some of the larger disks can be found in more complex magnetization configurations [Fig. 7(b)]. For single disks, the field stability of the vortex state decreases as the disk radius increases and it also becomes easier to obtain multiple vortices trapped in a single disk. For multilayer disks interlayer flux closure can further complicate the development of the magnetization state. A simulation of the remanent state for the largest (2.5 μm-diameter) disk in Fig. 7(b) confirms that complex (metastable) multivortex states are possible for larger diameters due to the comparably small contribution of the exchange energy. Such remanent multivortex states were simulated recently by a Monte Carlo technique for ultrathin disks.[27]

Figure 7(c) shows the PEEM images of the 20/20/20 nm disks. In these images, each disk is takes on essentially a single shade of gray, indicating that the magnetization state is

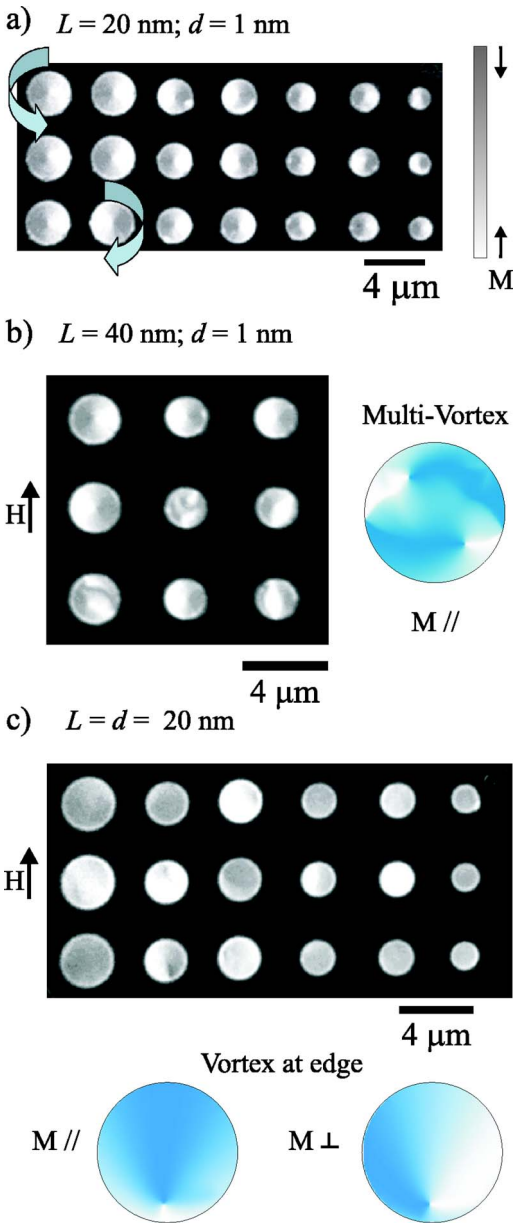

FIG. 7. (Color online) PEEM images showing the in-plane magnetization state of the top disk for Py/Cu/Py layers (diameters 1.2–2.5 μm) for thicknesses of (a) 20/1/20 nm, as fabricated, and (b) 40/1/40 nm and (c) 20/20/20 nm after saturating and returning to remanence. The grayscale map is proportional to the magnetization alignment with the in-plane direction of incidence of the x rays [parallel to direction of M shown in (a)]. Images of the as-fabricated sample with $d=1$ nm (a) show that all of the trilayer dots support a vortex magnetization state. After saturating and returning to zero field vortices are still observed, however, some of the larger dots are found in more complex multi-vortex/multi-domain states, as shown in (b). Simulations ("multi-vortex") of the remanent state from saturation show similarly complex magnetization states for the largest disks, where dark and light represent positive and negative saturation, respectively. For the dots in (c), the simulations indicate that one layer should be virtually single domain, i.e., featureless contrast, with some curling of the magnetization near the edges, while the other layer supports a vortex right at the edge (as shown), which will lead to some contrast near the dot edge.

predominantly uniform. This could be indicative of a flux-closure SD state. Indeed, the fact that the disks do not remain uniformly magnetized along the direction of the applied field once it has been removed lends credibility to the hypothesis that the lower layer is not magnetized in the same direction as the upper. The variation on the SD state remanent state suggested by the simulations for this geometry ($L=d=20$ nm) may also explain the observed images. The simulations show a state where one layer is SD with some curling, while the other supports a vortex right at the edge of the disk with the majority of the magnetization of that disk antiparallel to that of the other. Several disks show a change in coloration near the edge, and one resembles the perpendicular component of the edge-vortex magnetization, while other disks are perfectly uniform, all of which are consistent with the simulated state.

CONCLUSIONS

Experimentally measured hysteresis loops and PEEM images provide evidence consistent with the existence of a double vortex magnetization state in trilayer disks, that is, a state where two magnetic disks separated by a nonmagnetic spacer each support single vortices. The magnetic phase diagram based on analytical calculations of the lowest energy state shows a reduction in phase space of the vortex state due to flux closure between the layers, however, the simulations and experimental results indicate that the accessibility of the lowest energy state can also be a significant factor in determining both the remanent state and the reversal mechanism. The PEEM images for the larger disks (2.5 μm) also indicate that the magnetic properties may become more difficult to predict as the radius is increased due to the formation of more complicated multidomain states. The PEEM results confirm that the top layers of many of these structures support the vortex magnetic state while the hysteresis measurements for a 1-nm Cu spacer suggest a vortex reversal mechanism. Analytic predictions of the magnetic susceptibility also agree qualitatively with the experimental and simulation results. The numerical simulations suggest that the lower disk should support a vortex of opposing chirality, however, further experiments are necessary to confirm the state of the bottom layer.

ACKNOWLEDGMENTS

We thank M. Grimsditch for stimulating discussions and L. Ocola and R. Divan for support with e-beam patterning. K. B. thanks the Natural Sciences and Engineering Research Council (NSERC) of Canada for support. Work at Argonne was supported by the U.S. Department of Energy, BES Material Sciences under Contract No. W-31-109-ENG-38 and at Berkeley by the U.S. Department for Energy under Contract No. DE-AC0376SF00098.

*Corresponding author. Electronic address: buchanan@anl.gov

[1] K. Yu. Guslienko, V. Novosad, Y. Otani, H. Shima, and K. Fukamichi, Phys. Rev. B **65**, 024414 (2002).
[2] V. Novosad, K. Yu. Guslienko, H. Shima, Y. Otani, S. G. Kim, K. Fukamichi, N. Kikuchi, O. Kitakami, and Y. Shimada, Phys. Rev. B **65**, 060402 (2002).
[3] R. P. Cowburn, D. K. Koltsov, A. O. Adeyeye, M. E. Welland, and D. M. Tricker, Phys. Rev. Lett. **83**, 1042 (1999).
[4] C. A. Ross, M. Hwang, M. Shima, J. Y. Cheng, M. Farhoud, T. A. Savas, H. I. Smith, W. Schwarzacher, F. M. Ross, M. Redjdal, and F. B. Humphrey, Phys. Rev. B **65**, 144417 (2002).
[5] T. Shinjo, T. Okuno, R. Hassdorf, K. Shigeto, and T. Ono, Science **289**, 930 (2000).
[6] A. Fernandez and C. J. Cerjan, J. Appl. Phys. **87**, 1395 (2000).
[7] L. D. Buda, I. L. Prejbeanu, M. Demand, U. Ebels, and K. Ounadjela, IEEE Trans. Magn. **37**, 2061 (2001).
[8] J. Shibata and Y. Otani, Phys. Rev. B **70**, 012404 (2004).
[9] M. Natali, I. L. Prejbeanu, A. Lebib, L. D. Buda, K. Ounadjela, and Y. Chen, Phys. Rev. Lett. **88**, 157203 (2002).
[10] M. Grimsditch, P. Vavassori, V. Novosad, V. Metlushko, H. Shima, Y. Otani, and K. Fukamichi, Phys. Rev. B **65**, 172419 (2002).
[11] V. Novosad, M. Grimsditch, J. Darrouzet, J. Pearson, S. D. Bader, V. Metlushko, K. Yu. Guslienko, Y. Otani, H. Shima, and K. Fukamichi, Appl. Phys. Lett. **82**, 3716 (2003).
[12] G. Reiss, L. van Loyen, T. Lucinski, D. Elefant, H. Bruckl, N. Mattern, R. Rennekamp, and W. Ernst, J. Magn. Magn. Mater. **184**, 281 (1998).
[13] K. Yu. Guslienko, K. S. Buchanan, S. D. Bader, and V. Novosad, Appl. Phys. Lett. **86**, 223112 (2005).
[14] S. T. Chui, Phys. Rev. B **55**, 3688 (1997).
[15] ZEP-520A is a high sensitivity e-beam resist of positive tone produced by Nippon Zeon Co. (http://www.zeon.co.jp). ZEP consists of a copolymer of—chloromethacrylate and—methalstyrene.
[16] S.-B. Choe, Y. Acremann, A. Scholl, A. Bauer, A. Doran, J. Stohr, and H. A. Padmore, Science **304**, 420 (2004).
[17] A. Thompson *et al.*, X-Ray Data Booklet, LBNL/PUB-490 Rev. 2 (2001).
[18] W. Scholz, K. Yu. Guslienko, V. Novosad, D. Suess, T. Schrefl, R. W. Chantrell, and J. Fidler, J. Magn. Magn. Mater. **266**, 155 (2003).
[19] N. A. Usov and S. E. Peschany, J. Magn. Magn. Mater. **118**, L290 (1993); Fiz. Met. Metalloved. **12**, 13 (1994).
[20] K. Yu. Guslienko and V. Novosad, J. Appl. Phys. **96**, 4451 (2004).
[21] A. Aharoni, J. Appl. Phys. **68**, 2892 (1990).
[22] K. Metlov and K. Yu. Guslienko, J. Magn. Magn. Mater. **242–245**, 1015 (2002).
[23] H. F. Ding, A. K. Schmid, D. Li, K. Yu. Guslienko, and S. D. Bader, Phys. Rev. Lett. **94**, 157202 (2005).
[24] K. Yu. Guslienko and V. Novosad, Phys. Rev. Lett. **91**, 139701 (2003).
[25] LLG Micromagnetics Simulator™, M. R. Scheinfein, http://llgmicro.home.mindspring.com/.
[26] S. Savel'ev and F. Nori, Phys. Rev. B **70**, 214415 (2004).
[27] E. Yu. Vedmedenko, A. Ghazali, and J.-C. S. Levy, Phys. Rev. B **59**, 3329 (1999).